Journal of Thermal Analysis and Calorimetry, Vol. 83 (2006) 1, 253–260

HUMIDITY CONTROLLED THERMAL ANALYSIS
The effect of humidity on thermal decomposition of zinc acetylacetonate monohydrate

T. Arii [1*] *and A. Kishi* [2]

[1]Strategic Business Unit Thermal Analysis Group, Rigaku Corporation, 3-9-12 Matsubara, Akishima, Tokyo 196-8666, Japan
[2]Application center, Rigaku Corporation, 3-9-12 Matsubara, Akishima, Tokyo 196-8666, Japan

The low temperature formation of crystalline zinc oxide via thermal decomposition of zinc acetylacetonate monohydrate $C_{10}H_{14}O_4Zn{\cdot}H_2O$ was studied by humidity controlled thermal analysis. The thermal decomposition was investigated by sample-controlled thermogravimetry (SCTG), thermogravimety combined with evolved gas analysis by mass spectrometry (TG-MS) and simultaneous differential scanning calorimetry and X-ray diffractometry (XRD-DSC). Decomposition of $C_{10}H_{14}O_4Zn{\cdot}H_2O$ in dry gas by linear heating began with dehydration around 60°C, followed by sublimation and decomposition above 100°C. SCTG was useful because the high-temperature parallel decompositions were inhibited. The decomposition changed with water vapor in the atmosphere. Formation of ZnO was promoted by increasing water vapor and could be synthesized at temperatures below 100°C. XRD-DSC equipped with a humidity generator revealed that $C_{10}H_{14}O_4Zn{\cdot}H_2O$ decomposed directly to the crystalline ZnO by reacting with water vapor.

Keywords: *humidity, SCTG, TG-MS, thermal analysis, XRD-DSC, zinc acetylacetonate, zinc oxide*

Introduction

Thermal decomposition of inorganic or organic crystalline salt hydrates is an important class of reactions that should be studied for a variety of potential applications to ceramic industries. For instance, metal-organic salts have been widely used in various fields such as precursor materials for the fine particle of various metal oxide powders or thin-film fabrication so that it may be represented by sol–gel process and/or spray pyrolysis method.

The zinc oxide (ZnO) is expected as charges of the next generation electronic luminescence device materials, such as solar cell, transparent electric-conduction film as electrode of liquid-crystal screen, UV emitting diode and UV laser, etc. These various applications of ZnO are due to the specific chemical, surface and microstructural properties of ZnO. In general, such applications involve thin oxide films and past experience has shown that zinc oxide properties are significantly dependent on sample history and method of preparation. For example, anhydrous zinc acetate has been shown to be a suitable organometallic alternative to the alkyl zinc precursors [1] for ZnO film growth by chemical vapor deposition (CVD), and is used as the source material for ZnO films grown by atomic layer epitaxy (ALE) [2] and by splay pyrolysis [3, 4]. Musiæ *et al.* [5] reported that ZnO powders were synthesized using the decomposing urea process and crystallization from the suspensions obtained by abrupt mixing of $Zn(NO_3)_2$ and NH_4OH solutions. Audebrand *et al.* [6] investigated the early stages of ZnO formation by thermal decomposition of zinc nitrate, -oxalate, -hydroxide, -carbonate or -acetate. The chemical nature of these precursors influenced the formation of ZnO. Fine powder was prepared by hydrolysis of zinc acetylacetonate in a methanol-water mixture [7]. A significant difference of the particle shape between ZnO powders prepared at 25 and 80°C was revealed by transmission electron microscopy (TEM). Hohenberger and Tomandl [8] reported the sol–gel procedure for the preparation of ZnO-based varistors. Recently, the present authors focused on the effect of heating atmosphere for thermal process of metal carboxylates using novel thermal analyses equipped with a humidity generator [9]: sample-controlled thermal analysis (SCTA), simultaneous coupling measurement of thermogravimetric–differential thermal analysis and mass spectrometry (TG-DTA-MS) [10–12], and simultaneous measurement of X-ray diffractometry–differential scanning calorimetry (XRD-DSC) [13, 14]. To elucidate the underlying the thermal process in detail such complementary experimental thermal methodologies based upon hyphenated technology, satisfactorily improved the data interpretation.

As mentioned above, zinc acetylacetonate $C_{10}H_{14}O_4Zn{\cdot}H_2O$ has attracted much attention as one of the precursor materials for ZnO. It is therefore of interest to study this zinc acetylacetonate precursor, and

* Author for correspondence: t-arii@rigaku.co.jp

1388–6150/$20.00

Akadémiai Kiadó, Budapest, Hungary
Springer, Dordrecht, The Netherlands

decomposition to form ZnO. In the present work, we focused on low temperature synthesis of ZnO by using water vapor effect. The aim of this paper is to analyze in detail the thermal decomposition of $C_{10}H_{14}O_4Zn \cdot H_2O$ in dry gas and the atmospheres of controlled humidity, and especially to investigate the affect of water vapor on the change of reaction mechanism and the formation temperature of ZnO. The thermal behaviors of $C_{10}H_{14}O_4Zn \cdot H_2O$ under such different atmospheric conditions were investigated by means of humidity controlled thermal analyses of TG-DTA, TG-DTA-MS and XRD-DSC equipped with a humidity generator. The thermal pathway was remarkably influenced by changing the atmosphere and is discussed.

Experimental

Materials and methods

Material

The powder sample of zinc acetylacetonate monohydrate ($C_{10}H_{14}O_4Zn \cdot H_2O$, purity <98.0%, Wako Pure Chemical Industries, Ltd.) was the commercially available reagent without any further purification. An X-ray diffraction spectrum showed only crystalline $C_{10}H_{14}O_4Zn \cdot H_2O$ [15].

Methods

TG-DTA, was performed using a Rigaku Thermo Plus 8120D system equipped with SCTG mode. A sequence of experiments was carried out with a fully automated and computerized SCTG system [16], and the rate of mass loss was kept at an arbitrary constant value. The specimen mass of ca. 10 mg were weighed into an aluminum crucible, and were heated up to 550°C in dry air, high-purity dry helium (99.99%) or nitrogen (99.99%) and their atmospheres of controlled humidity, with a flow rate of 300 mL min^{-1}.

The spectra of the gaseous products evolved from the specimen in TG-DTA are simultaneously monitored with a quadrupole mass spectrometer (Model QP-5050A, Shimadzu). This mass spectrometer (MS) is connected to TG-DTA via a gas transfer tube with 3000 mm long stainless capillary tube of an internal diameter of 0.5 mm, whose the capillary internal surface is inactivated. Details of the TG-DTA-MS equipment are described elsewhere [17]. All of the transfer pathway was kept at 280°C to minimize condensation of the gaseous products evolved from the specimen. The acceleration voltage of the ionization for MS was fixed at potential of 70 eV. Detection mass region of m/z was fixed at 10–350. In a series of the simultaneous TG-DTA-MS experiments, to ignore desorption of any components adsorbed in the reference material such as α-Al_2O_3, only an empty crucible was used as reference.

The simultaneous measuring apparatus for XRD-DSC consisted of a specific heat flux type of DSC (Model Thermo Plus DSC8320, Rigaku) modified and combined with an X-ray diffractometer equipped with a two-dimensional high speed detector, D/tex-25, instead of a scintillation counter (XRD; Model RINT-Ultima III, Rigaku). Details of the XRD-DSC apparatus are described elsewhere [18]. The XRD-DSC measurements were carried out from ambient temperature to 200°C at a heating rate of 5°C min^{-1}. The specimen was mounted on a square aluminum container (7×7 mm and 0.25 mm in depth). A line shape X-ray source was operated at 50 kV and 40 mA and the data were collected in the range of $7° < 2\theta < 40°$ with an interval of 0.02° and a scan speed of 160° min^{-1}. With a temperature scan rate of 5°C min^{-1}, the change of sample temperature during each XRD scan corresponds to approx. 1°C, i.e. the XRD diagram obtained during each XRD scan expresses the mean spectrum of the temperature range of every 1°C. The θ and 2θ calibration was done using a silicon standard.

The special type of TG-DTA equipped with an electrical furnace surrounded by a specially designed water-jacket instead of conventional type of furnace was used in order to prevent condensation of water vapor. The isothermally controlled water into the water-jacket was supplied by a heating circulator (Model F25-MV, Julabo Labortechnik Gmbh, Seelbach, Germany). This modified type of TG-DTA apparatus was coupled with a humidity generator (Model HUM-1, Rigaku). The integrated humidity-controlled TG-DTA is described elsewhere [19]. The humidity generator can provide wet gases in the humidity range from 25°C–5%RH to 60°C–90%RH. Additionally, the present humidity generator was also coupled with the XRD-DSC apparatus.

Temperature calibration of TG-DTA and DSC was performed using pure metals of In, Sn and Pb.

Results and discussion

Thermal process in dry inert atmosphere

The typical TG-DTA-MS curves for $C_{10}H_{14}O_4Zn \cdot H_2O$ at a heating rate of 10°C min^{-1} in dry helium flow are shown in Fig. 1. The thermal process exhibited through several complex steps; a small amount of residue in the crucible was observed after the thermal analysis. The first mass loss of 6.3% up to 110°C was accompanied by an endothermic DTA peak at 82°C. The mass loss agreed approximately with the theoretical one corresponding to the thermal dehydration of one water molecule (6.40%).

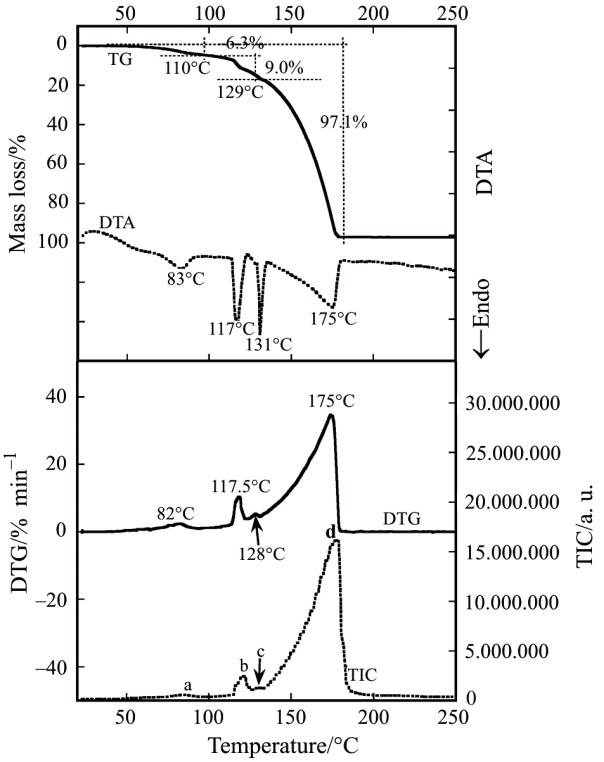

Fig. 1 Typical TG-DTA-MS results of $C_{10}H_{14}O_4Zn{\cdot}H_2O$ in dry helium flow at 10°C min^{-1}

After dehydration, the mass loss was divided into three reaction steps by the inflection points resolved from the DTG peaks. The total mass loss reaches over 97.1% at its final point (200°C) and a small amount of residual substance was presumably attributed to zinc oxide. On the other hand, the DTA curve indicated four endothermic peaks of 83, 117, 131 and 175°C, respectively. The first endothermic DTA peak showed a broad shape accompanying the mass loss, whereas the second and the third endothermic DTA peaks showed very sharp peaks, followed by a relatively broad fourth DTA peak. The shapes of the second and the third DTA peaks seem to be typical phase transition or melting phenomena, but the extrapolated onset-temperature (129.2°C) of the third DTA peak was slightly higher than the reported melting point (124–126°C) [20] of anhydrous zinc acetylacetonate; the difference may be attributed to the purity of the specimen. The TG, DTA and DTG curves were in good correspondence with the TIC curve that indicates sum of the ion current for all detected species. Figure 2 illustrates a comparison of the mass spectra obtained at the TIC peaks (a–d), where the mass spectra indicate the signal intensities after subtracting the background spectrum before heating. The observed mass spectra for the first to third TIC peaks seem to be similar to each other, suggesting the same components were formed concurrently. The intense ion sets of *m*/*z* 17 and 18 in the first TIC peak at 82°C (a) revealed that the evolved gas was mainly attributed to water vapor [21]. After dehydration, the mass spectra for the second (b) and the third (c) TIC peaks during the second mass loss of 9.0% consisted of the ion sets of 43, 58, 72, 85 and 100. By comparing with NIST-MS database, the original source could be identified as acetylacetone (*m*/*z* 15, 29, 43, 58, 72, 85 and 100) [22], suggesting the decomposition of the specimen. The other weak ions corresponded approximately to the fragmentation ions of acetylacetone, and water vapor. The mass spectrum for

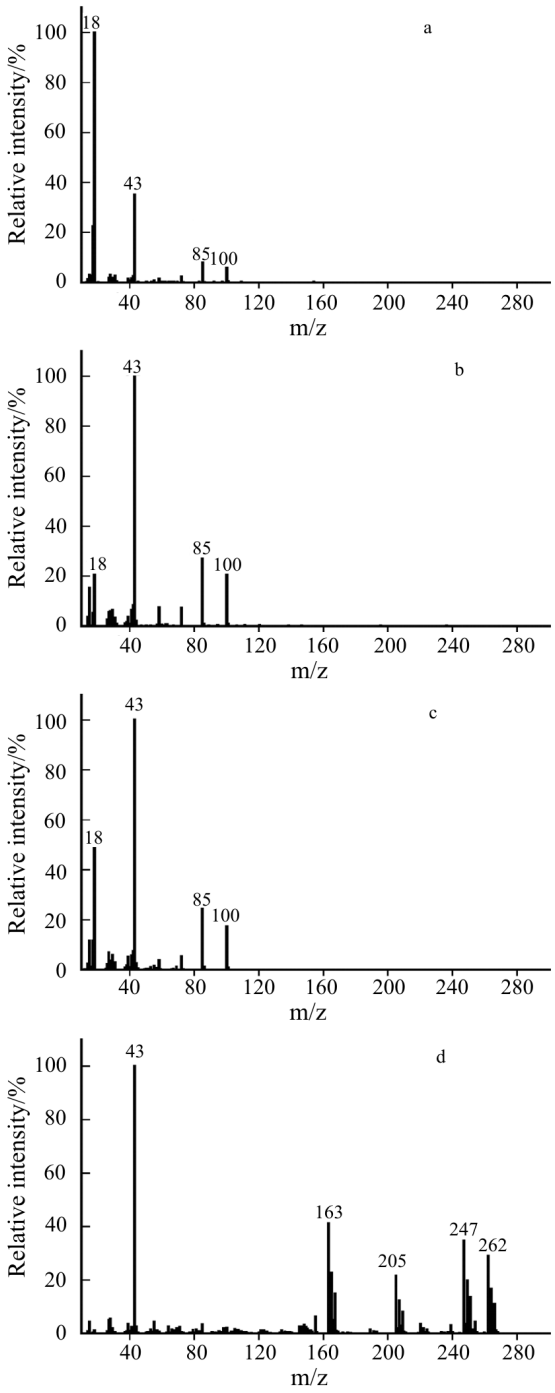

Fig. 2 Comparison of mass spectra obtained at a – 82, b – 117, c – 128 and d – 175°C in dry helium atmosphere

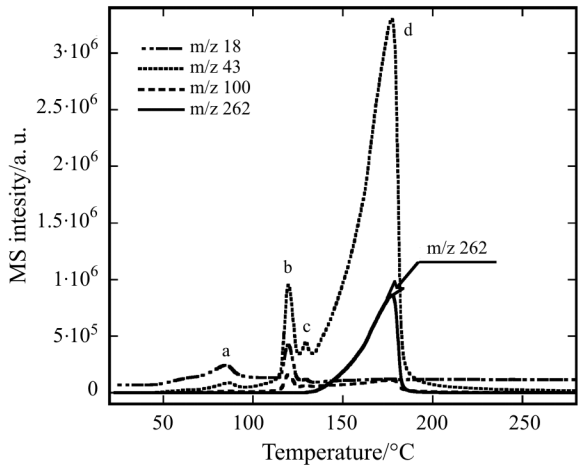

Fig. 3 Mass chromatograms of characteristic ions of *m*/*z* 18, 43, 100 and 262 obtained in dry helium atmosphere; *m*/*z* 18, H_2O^+; *m*/*z* 43, CH_3CO^+; *m*/*z* 100, $C_5H_8O_2^+$; *m*/*z* 262, $C_{10}H_{14}O_4Zn^+$

the final fourth TIC peak at around 175°C was quite different from those of other stages and consisted of higher ion sets. Simultaneous detection sets of *m*/*z* 43, 163, 205, 247 and 262 ions was attributed to the evolution of anhydrous zinc acetylacetonate [23], but the intensity of *m*/*z* 43 and 163 ions was fairly higher than expected from fragmentation of anhydrous zinc acetylacetonate. This fact suggested that anhydrous zinc acetylacetonate was not only evaporated, but also caused concurrently the thermal decomposition. Figure 3 illustrates the identified ion intensities of *m*/*z* 18(H_2O^+), 43(CH_3CO^+), 100($C_5H_8O_2^+$) and 262($C_{10}H_{14}O_4Zn^+$) as a function of the temperature. Evolution of anhydrous zinc acetylacetonate can be observed after the third TIC peak (c) around 130°C caused by fusion of the specimen.

Thermal process in the atmosphere of controlled humidity

Figure 4 shows a comparison of the TG-DTA curves for $C_{10}H_{14}O_4Zn{\cdot}H_2O$ at 5°C min^{-1} in nitrogen atmosphere of various partial pressures of water vapor (P_{H_2O}≤0.1, 1.7, 3.2, 6.1, 7.9, 11.9 and 15.9 kPa). The thermal process was strongly influenced by the partial pressure of water vapor in the atmosphere. With increasing the partial pressure of water vapor, the total mass loss decreased and the apparent mass loss curves shifted gradually toward lower temperature region. In the highest water vapor partial pressure (P_{H_2O}=15.9 kPa) condition, the total mass loss reached to 71.0% at 180°C and agreed satisfactorily with the theoretical mass loss to form zinc oxide (71.1%). Similarly, the profile of endothermic DTA curve changed dramatically and the reaction gradually took place in narrower temperatures with increasing the partial pressure of water vapor. In addition, it was noteworthy that the sharp second and the

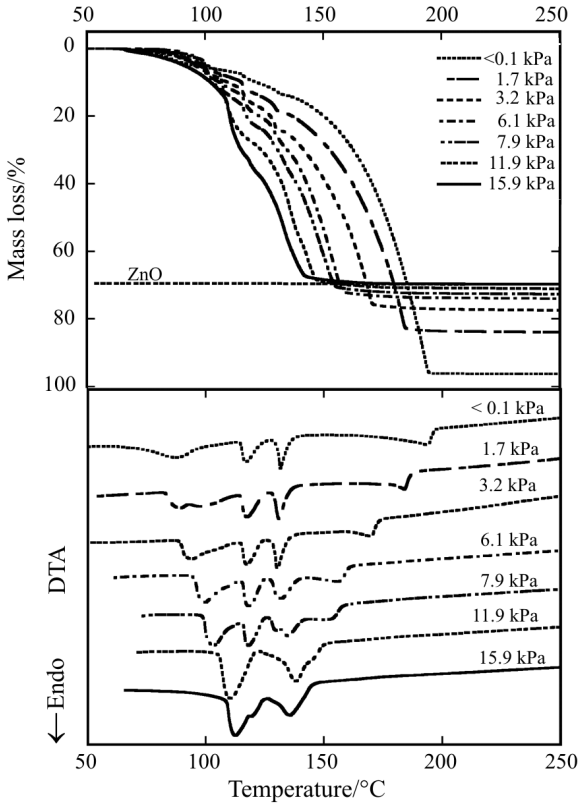

Fig. 4 Comparison of TG-DTA curves at 5°C min^{-1} for $C_{10}H_{14}O_4Zn{\cdot}H_2O$ in various partial pressures of water vapor (P_{H_2O}≤0.1, 1.7, 3.2, 6.1, 7.9, 11.9 and 15.9 kPa) in nitrogen atmosphere of controlled humidity

third endothermic DTA peaks disappeared under the atmospheres above the vapor partial pressure of 11.9 kPa. Similar experiments were made in various air atmospheres of controlled humidity. Therefore, the thermal process was basically identical with that in inert atmosphere of controlled humidity, i.e. the thermal process was changed by the partial pressure of water vapor, but not influenced by oxygen in the atmosphere. The total mass loss of 71.3% at the final point of 180°C in the partial pressure of water vapor (P_{H_2O} = 9.3 kPa) agreed satisfactorily with the theoretical mass loss corresponding to the formation of ZnO.

To elucidate the reaction process changing by introducing water vapor in the atmosphere, TG-DTA-MS observation made at 5°C min^{-1} in helium atmosphere of controlled humidity (P_{H_2O}=12 kPa) are shown in Fig. 5; the thermal behavior was similar with that obtained from nitrogen atmosphere of controlled humidity (P_{H_2O}=11.9 kPa). Both of DTG and TIC curves synchronized completely to each other, and the apparent peaks were observed through two steps; the mass loss began gradually around 70°C, followed by two clear TIC peaks at 109.1 and 134.4°C, and completed at 170°C. The total mass loss of 71.0% corresponds to the formation of ZnO. The mass spectra obtained at the both

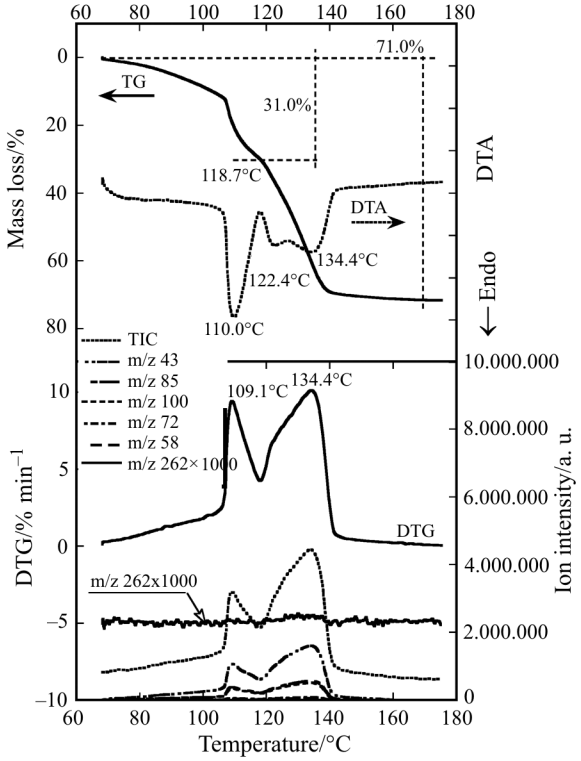

Fig. 5 Typical TG-DTA-MS results at 5°C min^{-1} for $C_{10}H_{14}O_4Zn{\cdot}H_2O$ in helium atmosphere of controlled humidity (P_{H_2O}=12 kPa); *m/z* 43, CH_3CO^+; *m/z* 58, $C_2H_6CO^+$; *m/z* 100, $C_5H_8O_2^+$; *m/z* 262, $C_{10}H_{14}O_4Zn^+$

TIC peaks (109.1 and 134.4°C) were completely identical to each other. Both are dominant by the spectra that consisted of *m/z* 43, 58, 72, 85 and 100, and the spectral pattern was assigned to only acetylacetone. Figure 5 represents also the characteristic ions of acetylacetone (*m/z* 43, 58, 72, 85 and 100) and molecular ion (*m/z* 262) of anhydrous zinc acetylacetonate as a function of temperature, together with the TIC. The spectral ion sets of acetylacetone synchronized completely to each other, but no ion sets of anhydrous zinc acetylacetonate was detected at all. These findings suggested that the atmosphere of controlled humidity was capable to prevent the sublimation of anhydrous zinc acetylacetonate and the formation of ZnO was effectively promoted with increasing the partial pressure of water vapor. The formation of ZnO was speculated by allowing anhydrous zinc acetylacetonate to react with water vapor and the thermal decomposition of $C_{10}H_{14}O_4Zn{\cdot}H_2O$ to ZnO in the atmosphere of controlled humidity proceeded apparently via two decomposition steps of acetylacetone.

To elucidate the above apparent two-step reactions, SCTG is useful because the high-temperature parallel reaction is inhibited by controlling the mass loss rate. Figure 6 illustrates a comparison of both the SCTG curves by a constant mass loss rate of 0.3% min^{-1} in the different heating atmospheres of dry air and in air of controlled humidity (P_{H_2O}=11.9 kPa). The SCTG

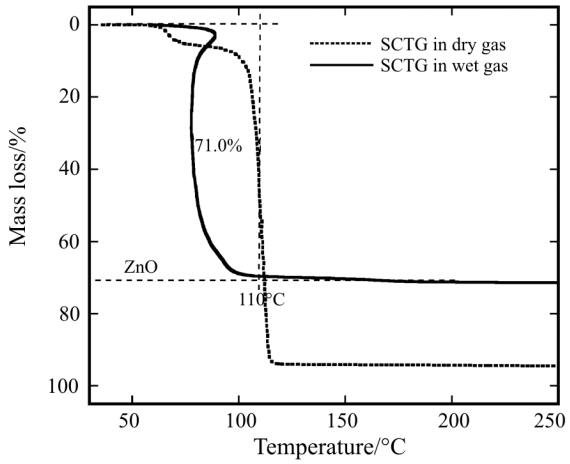

Fig. 6 Comparison of mass loss curves of $C_{10}H_{14}O_4Zn{\cdot}H_2O$ by SCTG of 0.3% min^{-1} between dry helium atmosphere and helium atmosphere of controlled humidity (P_{H_2O}=11.9 kPa)

curves were effectively shifted to lower temperature sides, but also the reaction temperature range became narrower than that of the TG. The thermal decomposition in dry atmosphere was simplified by two steps; the reaction began by dehydration around 60°C and completed isothermally around 110°C. No inflectional point was observed in course of the second reaction stage because SCTG may enable to prevent the additional reaction and to observe independently each reaction step. As the result, anhydrous zinc acetylacetonate was completely sublimated in dry gas atmosphere.

On the other hand, the SCTG in the atmosphere of controlled humidity was shown through a single-step and has a unique shape. The mass loss of 71.0% at the final point of 110°C agreed satisfactorily with the formation of ZnO. The mass loss profile directly revealed that a rate-determination step of the reaction is governed by the kinetic model of a nucleation and growth of the nuclei [24]. These findings also proposed that the atmosphere of high partial pressure of water vapor was capable to prevent the sublimation of anhydrous zinc acetylacetonate.

Finally, the thermal decomposition scheme in the atmosphere of controlled humidity (P_{H_2O}=11.9 kPa) by SCTG is simplified and can be proposed as follows.

$$Zn(CH_3COCHCOCH_3)_2{\cdot}H_2O \rightarrow ZnO + 2CH_3COCH_2COCH_3$$

By controlling the high partial pressure of water vapor with CRTG crystalline ZnO was synthesized at lower temperature region below 100°C.

XRD-DSC analysis

In order to prove formation of ZnO, it is important to recognize the products formed in the solid phase. The XRD-DSC at a heating rate of 5°C min^{-1} for

$C_{10}H_{14}O_4Zn{\cdot}H_2O$ in dry nitrogen atmosphere is shown in Fig. 7; the XRD diagram corresponding to each point on DSC curve with the same temperature range are represented on the left side. The DSC curve indicates that the thermal decomposition begins at around 80°C and ends at 200°C. The shape of the DSC curve corresponds approximately with that of the DTA in dry gas as shown in Fig. 4. Both the XRD and the DSC profiles suggest that the thermal process proceeds via several complicated reaction step. Also, an existence of five different solid phases revealed by changing the XRD diagrams. Figure 8 shows XRD diagrams for zinc acetylacetonate monohydrate (72.9°C) and the intermediate compounds at temperatures (109.5, 124.5, 137.4 and 191.5°C) corresponding to the end of each endothermic DSC event. The XRD diagrams obtained after the final endothermic reaction around 180°C have relatively weak crystalline peaks, indicating pure crystalline zinc oxide [25]. The XRD diagrams were gradually changed to anhydrate phase which completed the dehydration at 109.5°C, and the resulting phase agreed

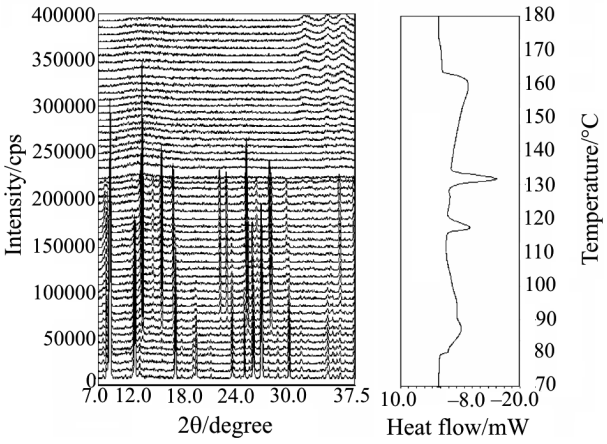

Fig. 7 XRD-DSC of $C_{10}H_{14}O_4Zn{\cdot}H_2O$ at 5°C min^{-1} in dry nitrogen atmosphere

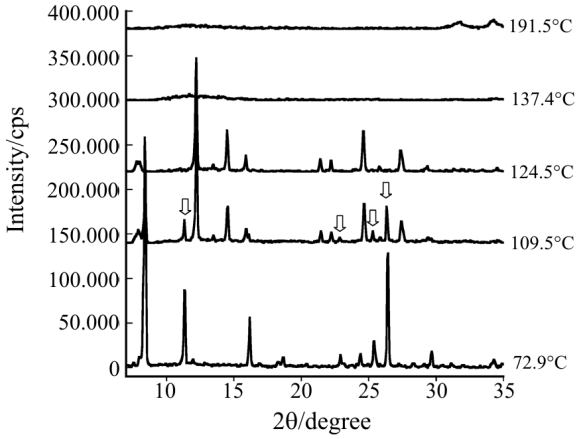

Fig. 8 Comparison of XRD diagrams at temperatures of 72.9, 109.5, 124.5, 137.4 and 191.5°C extracted from the end of each endothermic DSC peak

approximately with the reported XRD diagram of anhydrous zinc acetylacetonate [26]. From a comparison of the XRD patterns at 109.5 and 124.5°C before and after the second sharp endothermic peak, we can find a small difference between the XRD diagrams which suggested the structural change. The characteristic diffraction peaks inscribed by arrows in the XRD diagram of the anhydrate observed at 109.5°C were disappeared completely from the XRD diagram at 124.5°C after the DSC peak. This structural change may be attributed to the phase transition of anhydrous zinc acetylacetonate. On the other hand, the XRD diagram at 124°C was drastically changed by the third sharp endothermic phenomenon, and the resulting product at 134.5°C indicated no diffraction peaks, revealing the fusion of the specimen. After that, the diffraction peaks appeared gradually again after the peak of the fourth broad endothermic DSC which suggested a formation and growth of crystalline zinc oxide. From the results, it is proposed that the broad DSC phenomenon was mainly attributed to the parallel reactions of the evaporation and decomposition of anhydrous zinc acetylacetonate.

The XRD-DSC for $C_{10}H_{14}O_4Zn{\cdot}H_2O$ at a heating rate of 5°C min^{-1} in nitrogen atmosphere of controlled humidity (P_{H_2O}=11.9 kPa) is shown in Fig. 9. The complex endothermic DSC peaks may be speculated to the concurrent phase changes brought by overlapping phenomena of the exothermic and endothermic reactions. Also, the other hypothesis is that the thermal decomposition occurred through the formation of an intermediate product. From this viewpoint, the XRD diagrams simultaneously changed with DSC gave us very important information in regard to choice of the foregoing alternative hypotheses. Existence of two different solid phases can be clearly recognized in course of the thermal decomposition. The XRD diagrams of the $C_{10}H_{14}O_4Zn{\cdot}H_2O$ changed dramatically from the first DSC peak around 110°C, while the XRD diagrams of crystalline ZnO appeared gradually around the end of the first endothermic event. The integrated XRD intensities in the range of the diffraction angles characterizing the structural changes are represented together with the DSC

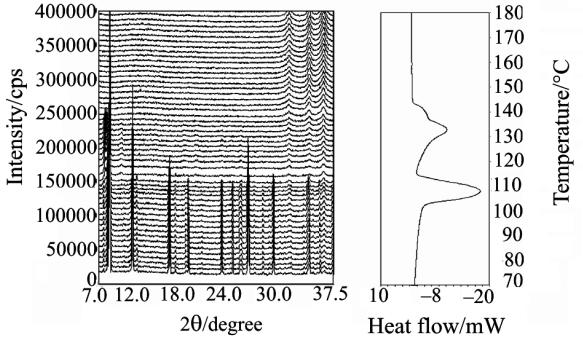

Fig. 9 XRD-DSC of $C_{10}H_{14}O_4Zn{\cdot}H_2O$ at 5°C min^{-1} in nitrogen atmosphere of controlled humidity (P_{H_2O}=11.9 kPa)

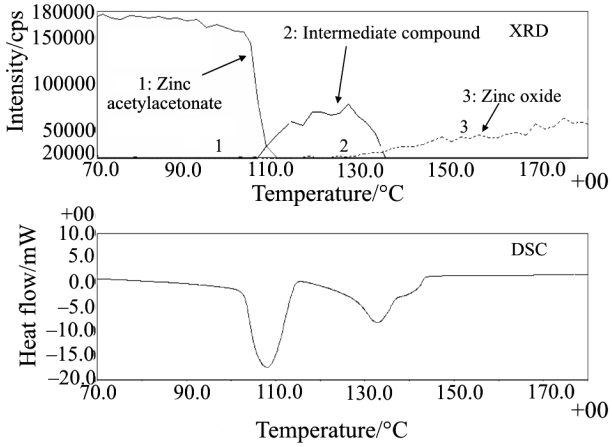

Fig. 10 Integrated intensity change of XRD peaks *vs*. temperature (upper) and DSC curve (lower) in humidity-controlled nitrogen atmosphere (P_{H_2O}=11.9 kPa); Curve 1: 11–12° (Zinc acetylacetonate), Curve 2: 31–33° (Zinc oxide)

curve in Fig. 10 as a function of temperature. The integrated intensity curve of XRD patterns of crystalline $C_{10}H_{14}O_4Zn{\cdot}H_2O$ between 11 and 12° shows a broad sigmoidal decay corresponding to the progress of the decomposition, while an increment of the integrated peak intensity in the diffraction angles between 31 and 33° reveals a concurrent formation and growth of crystalline zinc oxide. These trends could well explain that the thermal decomposition of $C_{10}H_{14}O_4Zn{\cdot}H_2O$ formed directly crystalline ZnO by reacting with the introduced water vapor into the atmosphere and crystalline ZnO was easily synthesized in the atmosphere of relatively high controlled humidity.

Conclusions

Thermal processes of $C_{10}H_{14}O_4Zn{\cdot}H_2O$ in dry gas and their atmospheres of controlled humidity were investigated by TG-DTA-MS, SCTG and XRD-DSC equipped with a humidity generator. The thermal process in dry gas atmosphere began with a single-step dehydration at ~110°C, followed by the complicated sequential and parallel reactions including phase transition, fusion, evaporation and decomposition of anhydrous zinc acetylacetonate. TG-DTA-MS in dry gas indicated clearly that the decomposition of anhydrous zinc acetylacetonate occurred together with evaporation of the specimen because evolution of acetylacetone and anhydrous zinc acetylacetonate were simultaneously detected. XRD-DSC in dry gas revealed that anhydrous zinc acetylacetonate occurred by phase transition around 120°C, followed by fusion around 130°C. A small amount of crystalline ZnO phase was detected as the residual substance. SCTG in dry gas revealed that anhydrous zinc acetylacetonate was completed by the sublimation of the specimen around 110°C without the decomposition so that the decomposition provided more simplified information to understand the reaction mechanism.

On the other hand, thermal process of anhydrous zinc acetate is strongly influenced by the partial pressure of water vapor in the atmosphere and the formation of ZnO accelerated with increasing the partial pressure of water vapor. TG-DTA-MS and XRD-DSC in the atmosphere of high controlled humidity revealed that $C_{10}H_{14}O_4Zn{\cdot}H_2O$ decomposes via the two-step mass losses accompanying the evolution of acetylacetone without the dehydration. However, the thermal decomposition of $C_{10}H_{14}O_4Zn{\cdot}H_2O$ in the atmosphere of high controlled humidity by heating condition of SCTG was simply indicated via a single-step ZnO formation and crystalline ZnO could be synthesized below 100°C.

These results demonstrated that humidity controlled thermal analyses such as TG-DTA-MS, SCTG and XRD-DSC equipped with a humidity generator are indispensable tools for determining the decomposition mechanism in sufficient detail to understand complicated thermal processes during syntheses of advanced ceramics materials. Especially, the synthesis of metal oxides via thermal decomposition of metal-organic precursors by using the atmosphere of controlled humidity will become effective in various fields as a kind of low temperature synthesis.

References

1 A. P. Roth and D. F. Williams, J. Appl. Phys., 52 (1981) 6685.
2 M. Tammenma, T. Koskinen, L. Hiltunen, M. Leskela and L. Niinesto, Thin Solid Films, 124 (1985) 125.
3 A. Ghosh and S. Basu, Mater. Chem. Phys., 27 (1991) 45.
4 S. A. Studenikin, N. Golego and M. Cocivera, J. Appl. Phys., 83 (1998) 2104.
5 S. Musić, D. Dragčević, M. Maljković and S. Popović, Mater. Chem. Phys., 77 (2002) 521.
6 N. Audebrand, J.-P. Auffrédic and D. Louér, Chem. Mater., 10 (1998) 2450.
7 K. Kamata, H. Hosono, Y. Maeda and K. Miyokawa, Chem. Lett., (1984) 2021.
8 G. Hohenberger and G. Tomandl, J. Mater. Res., 7 (1992) 1532.
9 T. Arii and A. Kishi, Thermochim. Acta, 400 (2003) 175.
10 R. Campostrini, G. D'Andrea, G. Carturan, R. Ceccato and G. D. Soraru, J. Mater. Chem., 6 (1996) 585.
11 J. J. Morelli, J. Anal. Appl. Pyrolysis, 18 (1990) 1.
12 T. Ozawa, T. Arii and A. Kishi, Thermochim. Acta, 352–353 (2000) 177.
13 T. Arii, A Kishi and Y. Kobayashi, Thermochim. Acta, 325 (1999) 151.
14 H. Yoshida, Thermochim. Acta, 267 (1995) 239.
15 Entry No. 41–1634, ICDD (zinc acetylacetonate hydrate, $C_{10}H_{14}O_4Zn{\cdot}H_2O$).

16 T. Arii, K. Terayama and N. Fujii, J. Thermal Anal., 47 (1996) 1649.
17 T. Arii, T. Senda and N. Fujii, Thermochim. Acta, 267 (1995) 209.
18 A. Kishi, M. Otuka and Y. Matsuda, Colloids and Surfaces B: Biointerfaces, 25 (2002) 281.
19 T. Arii, A. Kishi and Y. Sawada, J. Therm. Anal. Cal., 78 (2004) 639.
20 Aldrich reagent's chemical database, Product code # 038, CAS# 1402-63-6.
21 Entry No. 7, NIST 107 (water, H_2O).
22 Entry No. 19843, NIST 107 (acetylacetone, $C_5H_8O_2$).
23 Entry No. 12767, NIST 107 (zinc acetylacetonate, $C_{10}H_{14}O_4Zn$).
24 T. Arii and N. Fujii, J. Anal. Appl. Pyrolysis, 39 (1997) 129.
25 Entry No. 36–1451, ICDD (zinc oxide, ZnO).
26 Entry No. 23–1970, ICDD (zinc acetylacetonate, $C_{10}H_{14}O_4Zn$).

Received: January 27, 2005
In revised form: April 13, 2005

DOI: 10.1007/s10973-005-6921-3